Solar-blind ultraviolet photodetector based on $(LaAlO_3)_{0.3}$-$(SrAl_{0.5}Ta_{0.5}O_3)_{0.7}$ single crystal

Jian-yu Du, Chen Ge, Jie Xing, Jian-kun Li, Kui-juan Jin, Jing-ting Yang, Hai-zhong Guo, Meng He, Can Wang, Hui-bin Lu, and Guo-zhen Yang

Citation: AIP Advances **7**, 035302 (2017);

View online: https://doi.org/10.1063/1.4978053

View Table of Contents: http://aip.scitation.org/toc/adv/7/3

Published by the American Institute of Physics

Articles you may be interested in

Self-driven visible-blind photodetector based on ferroelectric perovskite oxides
Applied Physics Letters **110**, 142901 (2017); 10.1063/1.4979587

Self-powered sensitive and stable UV-visible photodetector based on $GdNiO_3$/Nb-doped $SrTiO_3$ heterojunctions
Applied Physics Letters **110**, 043504 (2017); 10.1063/1.4974144

Multiple temperature sensors embedded in an ultrasonic “spiral-like” waveguide
AIP Advances **7**, 035201 (2017); 10.1063/1.4977965

Feasibility study of SWIR light absorption enhancement in PbS and PbSe nano-structure layers using surface plasmon polariton
AIP Advances **7**, 035001 (2017); 10.1063/1.4977744

A computational study of flow past three unequal sized square cylinders at different positions
AIP Advances **7**, 035303 (2017); 10.1063/1.4977971

Mathematical model of a novel small magnetorheological damper by using outer magnetic field
AIP Advances **7**, 035114 (2017); 10.1063/1.4978866

Solar-blind ultraviolet photodetector based on $(LaAlO_3)_{0.3}$-$(SrAl_{0.5}Ta_{0.5}O_3)_{0.7}$ single crystal

Jian-yu Du,[1,2] Chen Ge,[1,a] Jie Xing,[2] Jian-kun Li,[1] Kui-juan Jin,[1,a] Jing-ting Yang,[1] Hai-zhong Guo,[1] Meng He,[1] Can Wang,[1] Hui-bin Lu,[1] and Guo-zhen Yang[1]

[1]*Beijing National Laboratory for Condensed Matter Physics, Institute of Physics, Chinese Academy of Science, Beijing 100190, People's Republic of China*

[2]*School of Science, China University of Geosciences, Beijing 100083, People's Republic of China*

(Received 18 January 2017; accepted 22 February 2017; published online 2 March 2017)

A solar-blind ultraviolet photodetector based on perovskite $(LaAlO_3)_{0.3}$-$(SrAl_{0.5}Ta_{0.5}O_3)_{0.7}$ (LSAT) single crystal has been fabricated. The Deep Ultra Violet (DUV)/Ultra Violet (UV) (200 versus 290 nm) ratio is more than three orders of magnitude under the applied bias voltage 200 V. Under illumination at 200 nm, the responsivity of this ultraviolet photodetector reaches 4 mA/W at 200 V bias. The corresponding quantum efficiency and detectivity are 2.76% and 1×10^{11} cm·Hz$^{0.5}$/W, respectively. The ultrafast response with a rise time of 563 ps and full width half maximum (FWHM) of 1.085 ns is obtained. The high sensitivity, ultrafast response speed, and good signal-to-noise ratio demonstrate that the LSAT photodetector could be a promising candidate as the solar-blind ultraviolet photodetector. © *2017 Author(s). All article content, except where otherwise noted, is licensed under a Creative Commons Attribution (CC BY) license (http://creativecommons.org/licenses/by/4.0/).* [http://dx.doi.org/10.1063/1.4978053]

I. INTRODUCTION

Ultraviolet (UV) photodetectors have attracted much attention for their wide applications in the fields of communication, flame detection, missile tracking, ozone holes monitoring, corona detection, and chemical or biological agent sensing.[1–4] UV photodetectors consist of visible-blind (below 400 nm) ultraviolet photodetector[5,6] and solar-blind ultraviolet (below 280 nm) photodetector.[7,8] Because most photons in the wavelength shorter than 280nm have been strongly absorbed by the stratospheric ozone layer,[9] solar-blind ultraviolet photodetectors, compared to visible-blind ultraviolet photodetectors, show superior advantages with lower false alarm rate and higher sensitivity under sun or room illumination. Recently, solar-blind ultraviolet photodetector based on wide bandgap semiconductors, such as diamond,[1,2,10] BN,[11,12] AlGaN,[7] Ga_2O_3,[13–15] have been widely investigated. However, the fabrication processes for the photodetectors above are expensive and complex. In recent years, perovskite oxides with wideband gap, which have strong stability against harsh environment,[16,17] have attracted much attention, due to their excellent photoelectric property and potential ultrafast performance.[18–22]

In this work, we employed the commercial LSAT (001) single crystal (MTI corporation) to fabricate a solar-blind photodetector. The LSAT single crystal, as one of the perovskite oxides, has a wide bandgap of 4.96eV, so it may be a candidate for solar-blind detection. The photodetector shows a maximum response under the illumination of 200 nm wavelength, and the responsivity of the photodetector is about 4 mA/W. The response rejection ratio (R(204 nm)/R(280 nm)) is more than three orders of magnitude under the applied bias 200 V. Importantly, the photodetector exhibits an ultrafast response to UV light. The high rejection ratio, low noise current, and ultrafast response demonstrate that LSAT is a promising material to fabricate solar-blind ultraviolet photodetectors.

[a]Corresponding author to whom correspondence should be addressed; E-mail: gechen@iphy.ac.cn or kjjin@iphy.ac.cn

 © Author(s) 2017

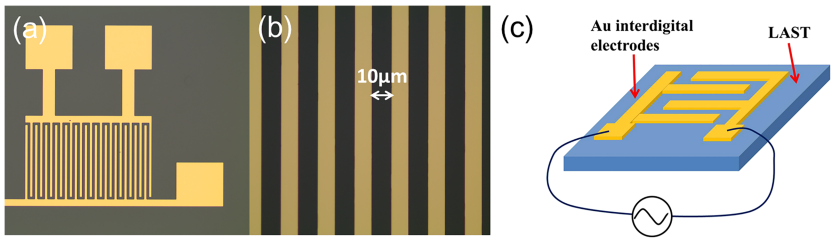

FIG. 1. (a) Optical images of the interdigital electrodes with finger widths of 10μm on LSAT, (b) Magnification of the interdigital electrodes, (c) Schematic diagram of the LSAT photodetector with interdigital electrodes.

II. EXPERIMENTAL METHOD

The size of LSAT wafer is 10 mm × 10 mm with a thickness of 0.5 mm. Using the standard photolithography and thermal evaporation techniques, we fabricated interdigitated electrodes on LSAT crystals. Here, we employed Au as the electrodes. The photographs of the electrode patterns are exhibited in figure 1(a). Figure 1(b) is the magnification of the electrode pattern. A series of interdigitated electrodes with different finger spacings of 10, 20, and 30 μm were fabricated to investigate the effect of the finger spacing on the photodetection characteristic. Two platinum wires were connected to the interdigitated electrodes for electrical measurements. Figure 1(c) exhibits the schematic diagram of LSAT photodetector. The photoelectric signals of the photodetector were measured with a semiconductor parameter analyzer (Keithley 4200). The spectral responsivity was measured using a monochromator combined with a lock-in amplifier (Stanford SR830), and laser-driven light source (EQ-99X) was utilized as the light source. A 2.5 GHz digital oscilloscope (Tektronix TDS7254B) and an actively-passively mode-locked Nd:YAG laser (EKSPLA PL2210A) were used to characterize the ultrafast photoelectric response of LSAT photodetector.

III. RESULTS AND DISCUSSION

The spectral responsivity of the LSAT photodetector with a finger width of 10 μm is displayed in figure 2(a). Inset of figure 2(a) is a logarithm analysis of responsivity for clearly displaying the response rejection ratio. The applied voltages were 50 (black), 100 (red), 150 (green), and 200 V (blue), respectively. There is an obvious spectral responsivity under the light illumination with wavelengths ranging from 200 to 250 nm, while there is almost no response to the light with wavelengths longer than 250 nm. Maximum of responsivity locating at about 200nm were 0.94, 2.01, 3.13 and 4.28 mA/W at 50, 100, 150 and 200 V, respectively. A sharp cutoff appeared at about 250 nm, which is approximately the same value of the absorption edge of LSAT as shown in figure 2(b). The photon

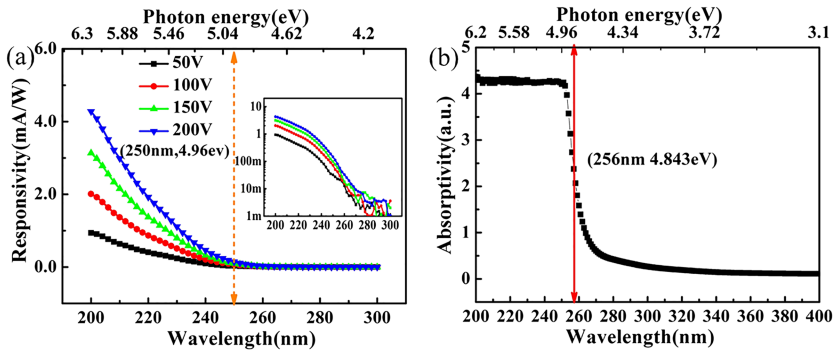

FIG. 2. (a) Spectral response of the LSAT photodetector with a finger width of 10μm at 50 (black), 100 (red), 150 (green), 200 (blue) bias, Inset is a replot of responsivity curve in a logarithmic scale, (b) Absorption spectra of LSAT single crystal.

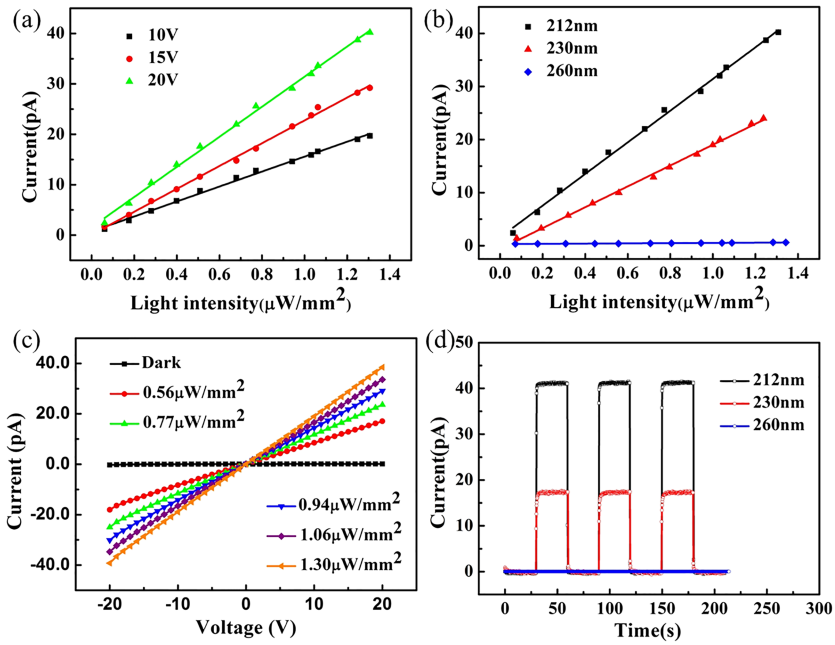

FIG. 3. (a) Photocurrent variation with the light intensity under illumination of 212 nm UV light at 10, 15, 20 V bias respectively, (b) Photocurrent variation with the light intensity under illumination of different wavelengths at 20 V bias, (c) I-V characteristics of detectors with different light intensity under illumination of 212 nm UV light, (d) Steady-state photoelectric response under different excitation wavelengths at 20 V.

energy that corresponds to the cutoff wavelength is 4.96eV, demonstrating a bandgap excitation process. The response rejection ratio (R(204 nm)/R(280 nm)) is more than three orders of magnitude under the applied bias voltage 200 V, indicating an intrinsic solar blindness. The responsivity of the LSAT photodetector increases with increasing the applied bias. This phenomenon can be understood as follows. A larger voltage will result in a higher electric field which can separate the photo-induced electron-hole pairs more easily and reduced the recombination of photo-carriers, thus more photo-carriers can been collected.[23]

Figure 3(a) shows the dependence of the photocurrent on the light intensity under the illumination of light with a wavelength 212 nm under various biases. It is found that the photocurrent has a good liner relationship with the light intensity and no photocurrent saturation phenomenon appeared from 0.06 to 1.306 μm/mm^2. Figure 3(b) displays the dependence of the photocurrent on the light intensity under various light wavelengths. All the photocurrents have a good linear relationship with the light intensity, and there is no photoelectric response under the illumination of the light wavelength 260 nm. Moreover, we also carried out investigations on the *I-V* characteristics of the photodetector under various light intensities, as shown in figure 3(c). The photocurrent increases with the applied bias under the different light intensity. At the same bias, the photocurrent increases with the increasing of light intensity. Figure 3(d) shows the steady-state photocurrents of the LSAT photodetector under the light illumination with wavelengths of 212, 230, and 260 nm, respectively. Obviously, the photocurrent strongly depends on the light illumination. In addition, the time response characteristic was investigated by the transient photocurrent method. The detector was operated under the illumination of a pulsed 230 nm laser with 15 ps duration, and a 2.5GHz digital oscilloscope was employed to collect the data. Figure 4 shows a transient response of the LSAT detector at 70 V bias. The rise time and FWHM are 563 ps and 1.085 ns, respectively. This result indicates an ultrafast photoelectric response of LSAT photodetector.

Figure 5 (a) shows the *I-V* characteristics of photo detectors with various finger widths. At the same bias of 20V, the photocurrent increases as the finger width decreases. In addition to the above performance indexes, we also investigate other important parameters. The quantum efficiency η, describing the capability of carriers generation, is an extraordinary factor for the photodetector.

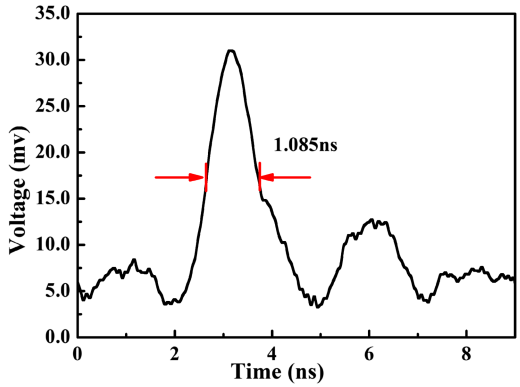

FIG. 4. Ultrafast photoelectric response of the LSAT detector with a finger width of 10 μm at 70V bias, measured by a 2.5 GHz oscilloscope, and a laser with pulse width of 25 ps.

$$\eta = R_i hc/\lambda q \tag{1}$$

where R_i is the responsivity, λ is the wavelength, h is Planck's constant, c is the light velocity, and q is the electron charge. The spectral response R_i can be evaluated by

$$R_i = I/(E \cdot A) \tag{2}$$

where I is photocurrent, E is light power density, and A is active area.

Detectivity D^* is one of the main parameters characterizing normalized signal-to-noise performance of detectors. There are some factors influencing the noise and further limits D^*: the shot noise from dark current, Johnson noise, and thermal fluctuation "flicker" noise. Here, the thermally limited mode may not be applied as the short noise is significant. Therefore, the D^* can be calculated by[24,25]

$$D^* = R_\lambda \sqrt{A}/(\frac{4k_bT}{R_{dark}} + 2qI_{dark})^{1/2} \tag{3}$$

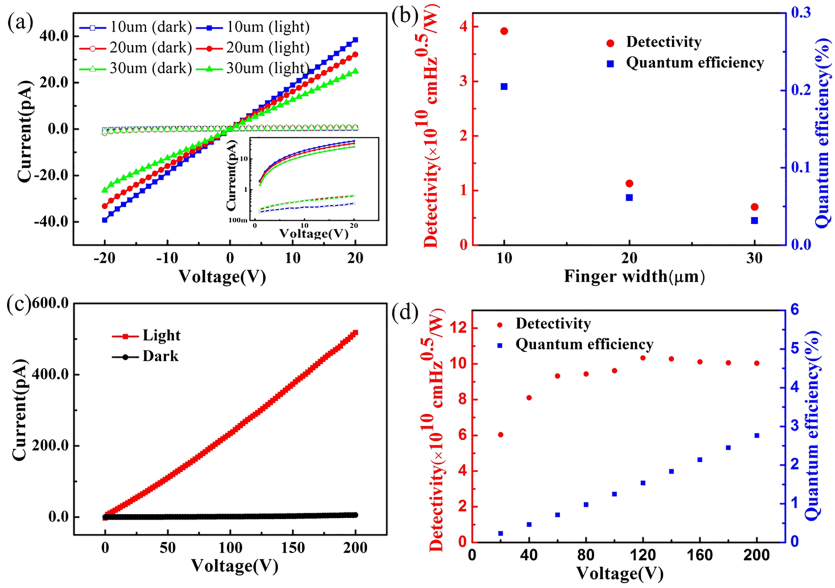

FIG. 5. (a) I-V characteristics of photo detectors with various finger widths, (b) Detectivity (red) and quantum efficiency (blue) variation with the finger width under illumination of 212nm at 20V bias, (c) I-V characteristics of detectors in dark and under 212nm illumination, (d) Detectivity (red) and quantum efficiency (blue) variation with voltage under illumination of 212nm.

where k_b is the Boltzman constant, T is the temperature, R_{dark} is the detector differential resistance. Here, q is electron charge, I_{dark} is the dark current, and R_λ is the responsivity at different wavelength, A is active area.

As shown in figure 5(b), at a 20V bias with a wavelength 212 nm, η of the photodetectors with different finger widths of 10, 20, and 30 μm are 0.2055 %, 0.0614 %, and 0.0317 %, respectively. The corresponding D^* of these photodetector are 3.92×10^{10}, 1.13×10^{10}, and 7×10^9 cm·Hz$^{0.5}$/W, respectively. Both the quantum efficiency and the detectivity increase with decreasing the finger widths. This can be understood as follows. Narrower finger width induces stronger electric field, which will promote the combination probability of the photo-generated carriers when they transport between electrodes.

Figure 5(c) shows the *I-V* curves of LSAT in dark and under the 212 nm radiation with the voltage ranging from 0 to 200V. The results show that the LSAT photodetector is stable on a wide range of biases (below 200V). Besides, at room temperature, the photodetector exhibits a very small dark current ~5.82 pA at 200V bias. This phenomenon is generally attributed to its high crystal quality. The D^* which corresponds to different voltage is also calculated and shown in figure 5(d), and the maximum value is about 1×10^{11} cm·Hz$^{0.5}$/W. The quantum efficiency almost grows linearly with the applied voltage.

In order to improve the photoelectric performance, we fabricated photodetectors with multiple cells connected in parallel. Figure 6(a) shows the *I-V* characteristics of the photodetector with various cells in parallel. It can be seen that the photocurrent increases with increasing the cell number. Moreover, the photocurrent ~143 pA of the photodetector with three cells in parallel increases more than three times compared with that ~38 pA of the photodetector with one cell. We also investigate the dependence of D^* on the cell numbers of the photodetector. As shown in figure 6(b), the corresponding D^* for photodetector with cell numbers of one, two, and three are 3.9×10^{10} cm·Hz$^{0.5}$/W, 5.1×10^{10} cm·Hz$^{0.5}$/W, and 6.1×10^{10} cm·Hz$^{0.5}$/W, respectively.

Figure 6(c) shows the steady-state photocurrent properties of the detector with different cell numbers. The photocurrent is recorded by Keithley 4200 under the illumination of a 212 nm light

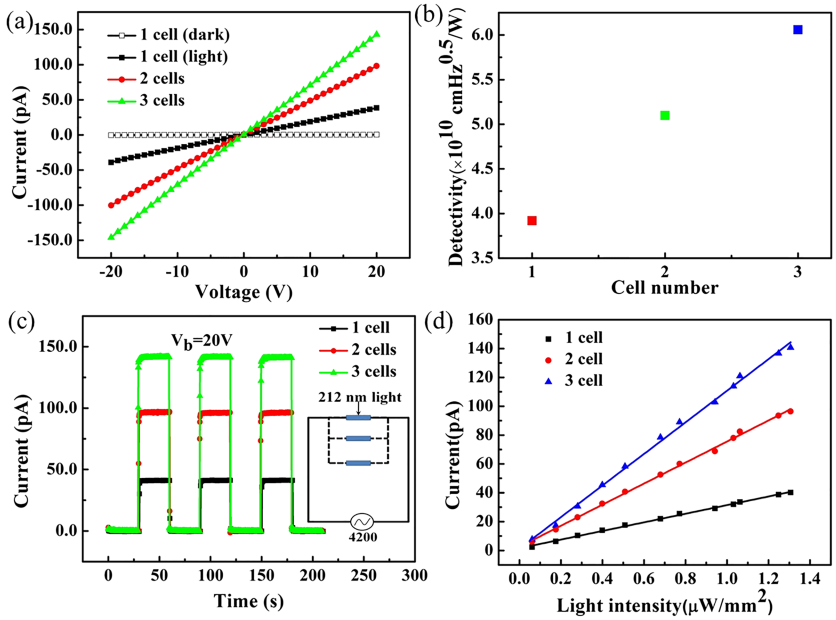

FIG. 6. (a) I-V characteristics of detectors with different interdigital electrode cell numbers under illumination of 212 nm UV light. Open data points are for dark currents and solid data points indicate photocurrents. (b) Detectivity variation with the cell number under illumination of 212nm at 20V bias. (c) Steady-state current response of the devices with different interdigitated electrode cell numbers under illumination of a 212 nm light at 20V bias. The power density is 1.306μw/mm^2. The inset shows the schematic circuit of measurement. (d) Photocurrent variation with the light intensity under illumination of 212 nm light with different cell number.

with an intensity of 1.306 μW/mm^2, and the applied bias is 20 V. From figure 6(c), it can be seen that the current is strongly dependent on the irradiation of light. The current is high when the light is on, while the current is low when the light is off. This reflects its good deep ultraviolet characteristic. The photocurrent increases from 41 pA to 141 pA, when the cell number increases from one to three. Figure 6(d) exhibits the dependence of the photocurrent of the LSAT photodetector on the light intensity of a 212nm light at 20 V bias, showing a favorable linear relationship between photocurrent and light intensity. All these results show that we can improve the performance of photodetector of LSAT through integrating multiple cells on the detector in parallel configuration.

IV. CONCLUSIONS

In conclusion, the solar-blind photodetector based on a LSAT single crystal has been fabricated and the photodetector characteristic has been investigated. The photodetector displays a high response rejection ratio with more than three orders of magnitude at ambient temperature and sharp cutoff wavelength is about 250 nm which is located in the solar-blind region. The photocurrent increases linearly with the applied bias and light intensity. This linear relationship keeps well when the voltage increases to 200V. The photodetector also exhibits a low dark current of 5.82 pA, an ultrafast response signal with a rise time of 563 ps, and detectivity D* of 1×10^{11} cmHz$^{0.5}$/W, under the illumination of a light with wavelength 212 nm. We also investigated LSAT photodetectors with multiple interdigital electrode cells connected in parallel, and found that the photocurrent response of the photodetectors can increase linearly with increasing the cell number. These results demonstrate that LSAT photodetectors have potential for the application in the solar blind photoelectric detecting.

ACKNOWLEDGMENTS

This work was supported by the National Hi-tech (R&D) project of China (No. 2014AA032607), the National Basic Research Program of China (Nos. 2014CB921001 and 2013CB328706), the Key Research Program of Frontier Sciences, CAS (No. QYZDJSSW-SLH020), and the National Natural Science Foundation of China (Nos. 11674385, 11404380, 11574365, 11474349, and 11104255), and the Strategic Priority Research Program (B) of the Chinese Academy of Sciences (No. XDB07030200) and Fundamental Research Funds for the Central Universities (Grant Nos. 53200859478 and 53200859128).

[1] A. BenMoussa, J. F. Hochedez, U. Schühle, W. Schmutz, K. Haenen, Y. Stockman, A. Soltani, F. Scholze, U. Kroth, V. Mortet, A. Theissen, C. Laubis, M. Richter, S. Koller, J. M. Defise, and S. Koizumi, Diamond and Related Materials **15**, 802 (2006).
[2] F. Spaziani, M. C. Rossi, S. Salvatori, G. Conte, and P. Ascarelli, Applied Physics Letters **82**, 3785 (2003).
[3] D. Y. Guo, Z. P. Wu, Y. H. An, X. C. Guo, X. L. Chu, C. L. Sun, L. H. Li, P. G. Li, and W. H. Tang, Applied Physics Letters **105**, 023507 (2014).
[4] X. Zhou, Q. Zhang, L. Gan, X. Li, H. Li, Y. Zhang, D. Golberg, and T. Zhai, Advanced Functional Materials **26**, 704 (2016).
[5] I. K. Sou, M. C. W. Wu, T. Sun, K. S. Wong, and G. K. L. Wong, Applied Physics Letters **78**, 1811 (2001).
[6] J. W. Tomm, B. Ullrich, X. G. Qiu, Y. Segawa, A. Ohtomo, M. Kawasaki, and H. Koinuma, Journal of Applied Physics **87**, 1844 (2000).
[7] D. Walker, V. Kumar, K. Mi, P. Sandvik, P. Kung, X. H. Zhang, and M. Razeghi, Applied Physics Letters **76**, 403 (2000).
[8] Z. G. Ju, C. X. Shan, D. Y. Jiang, J. Y. Zhang, B. Yao, D. X. Zhao, D. Z. Shen, and X. W. Fan, Applied Physics Letters **93**, 173505 (2008).
[9] L. Sang, M. Liao, and M. Sumiya, Sensors **13**, 10482 (2013).
[10] A. BenMoussa, U. Schühle, F. Scholze, U. Kroth, K. Haenen, T. Saito, J. Campos, S. Koizumi, C. Laubis, M. Richter, V. Mortet, A. Theissen, and J. F. Hochedez, Measurement Science and Technology **17**, 913 (2006).
[11] W. J. Zhang, Y. M. Chong, I. Bello, and S. T. Lee, Journal of Physics D: Applied Physics **40**, 6159 (2007).
[12] P. B. Mirkarimi, K. F. McCarty, and D. L. Medlin, Materials Science and Engineering: R: Reports **21**, 47 (1997).
[13] L. X. Qian, X. Z. Liu, T. Sheng, W. L. Zhang, Y. R. Li, and P. T. Lai, AIP Advances **6**, 045009 (2016).
[14] Z. Zhang, H. von Wenckstern, J. Lenzner, M. Lorenz, and M. Grundmann, Applied Physics Letters **108**, 123503 (2016).
[15] J. Du, J. Xing, C. Ge, H. Liu, P. Liu, H. Hao, J. Dong, Z. Zheng, and H. Gao, Journal of Physics D: Applied Physics **49**, 425105 (2016).
[16] Y. Guo, C. Liu, H. Tanaka, and E. Nakamura, The Journal of Physical Chemistry Letters **6**, 535 (2015).

[17] J. Xing, E. Guo, K. Jin, H. Lu, J. Wen, and G. Yang, Optics Letters **34**, 1675 (2009).
[18] H. Ni, S. Q. Zhao, and K. Zhao, Applied Optics **49**, 2635 (2010).
[19] E. Guo, J. Xing, H. Lu, K. Jin, J. Wen, and G. Yang, Journal of Physics D: Applied Physics **43**, 015402 (2010).
[20] K. Zhao, K. Jin, Y. Huang, S. Zhao, H. Lu, M. He, Z. Chen, Y. Zhou, and G. Yang, Applied Physics Letters **89**, 173507 (2006).
[21] J. Yang, C. Ge, K. Jin, H. Lu, and G. Yang, Applied Optics **55**, 2259 (2016).
[22] E. Guo, J. Xing, K. Jin, H. Lu, J. Wen, and G. Yang, Journal of Applied Physics **106**, 23114 (2009).
[23] L. Wang, K. Jin, J. Xing, C. Ge, H. Lu, W. Zhou, and G. Yang, Applied Optics **52**, 3473 (2013).
[24] M. Razeghi and A. Rogalski, Journal of Applied Physics **79**, 7433 (1996).
[25] W. Zhou, K. Jin, H. Guo, C. Ge, M. He, and H. Lu, Journal of Applied Physics **144**, 224503 (2013).